RESEARCH ARTICLE
SPACE PHYSICS

Earth and Planetary Physics
9: 711–718, 2025
doi: 10.26464/epp2025039

Modeling of the *Sq* geomagnetic field induced by tidal oscillations of the atmosphere

WenBo Li[1], DaLi Kong[1]*, HongBo Yao[2], and Hao Yan[2]

[1]Shanghai Astronomical Observatory, Chinese Academy of Sciences, Shanghai 200030, China;

[2]Macau Institute of Space Technology and Application, Macau University of Science and Technology, Macao 999078, China

Key Points:

- An *Sq* (solar quiet) geomagnetic field model is built based on the atmospheric thermal tide theory and electrodynamics.
- The model performance has been investigated using the Macau Science Satellite-1 measurements.
- The model sets a physics-based framework for *Sq* magnetic field modeling in future comprehensive geomagnetic field models.

Citation: Li, W. B., Kong, D. L., Yao, H. B., and Yan, H. (2025). Modeling of the *Sq* geomagnetic field induced by tidal oscillations of the atmosphere. *Earth Planet. Phys.*, *9*(3), 711–718. http://doi.org/10.26464/epp2025039

Abstract: The *Sq* (solar quiet) geomagnetic field is generated by the electric currents in the E-region of the ionosphere, driven by the atmospheric tides. It is a critical part of high-precision geomagnetic field modeling. Based on the classic thermal tide theory and atmospheric electrodynamics, this research, for the first time, developed an *Sq* geomagnetic field model that is directly built on the physical mechanism of the ionospheric dynamo, which is responsible for daily variations of the geomagnetic field. The performance in *Sq* geomagnetic field modeling was investigated using the Macau Science Satellite-1 (MSS-1) data. Our model can enhance the physics-based framework of comprehensive geomagnetic field modeling for the MSS-1 and ensuing missions.

Keywords: Macau Science Satellite-1; *Sq* geomagnetic field; atmospheric tides

1. Introduction

The geomagnetic field plays a significant role in both geoscientific research and practical applications. The investigation and utilization of the geomagnetic field rely on the precise measurements and physical modeling. The Macau Science Satellite-1 (MSS-1) mission launched in 2023 provides the unprecedentedly accurate geomagnetic measurements for the first time in China (Zhang K, 2023). A key step of the physical modeling is the decomposition of the geomagnetic field from various sources. With the geomagnetic measurements provided by MSS-1, many researches have focused on the separation and analysis of geomagnetic field, originated from different regions, including the Earth's liquid core (Yao HB et al., 2025a), the mantle and curst (Ren ZY et al., 2025a; Yao HB et al., 2025b), the ocean tides (Ren ZY et al., 2025b), and the magnetosphere (Wang YB et al., 2023).

In addition to the regions mentioned above, the ionosphere also contributes to the geomagnetic field. The Earth's ionosphere exhibits a complex conductivity structure mainly due to the solar radiation. The ionospheric currents, generated by the dynamo process on the dayside of the E-region of ionosphere from 90 km to 150 km in altitude, are responsible for the daily variations of the geomagnetic field that could be measured by MSS-1. The solar quiet (*Sq*) geomagnetic field is one of the most significant daily variations generated by the ionospheric currents (Matsushita, 1968; Campbell, 1989). The *Sq* geomagnetic field is enhanced near the magnetic equator due to the contributions of the equatorial electrojet (EEJ) (Chapman, 1951). The variations of ionospheric currents can also induce electric currents in the upper mantle (Schmucker, 1970), which generate an induced geomagnetic field that contributes to the daily variations of geomagnetic field. Besides the *Sq* geomagnetic field, another daily variation of the geomagnetic field is the lunar variation, denoted as *L*, that is also generated by the ionospheric dynamo and changes with the phase of the moon (Campbell, 1980). Yamazaki and Maute (2017) gives a thorough review on daily variations of the geomagnetic field caused by ionospheric dynamo currents.

As the strength of *Sq* geomagnetic field is usually on the order of a few tens of nano tesla (nT) at the altitute of LEO statellites, its contribution to the total geomagnetic measurements must be taken into account in high-precision geomagnetic field modeling. During the CHAMP and Swarm missions (Olsen et al., 2013), the Dedicated Ionospheric Field Inversion (DIFI) chain algorithm (Chulliat et al., 2013, 2016; Sabaka et al., 2020) has been developed to successfully separate and study the *Sq* geomagnetic field. Although the DIFI algorithm was built on the quasi-dipole symmetric basis functions (Richmond, 1995; Emmert et al., 2010) that reflect the conductivity structure of the ionospheric E-region (Sabaka et al., 2020), the physical mechanism of ionospheric

First author: W. B. Li, wli@shao.ac.cn
Correspondence to: D. L. Kong, dkong@shao.ac.cn
Received 10 MAR 2025; Accepted 24 MAR 2025.
First Published online 14 APR 2025.

dynamo was missing in the inversion of the *Sq* geomagnetic field.

The physical mechanism of the ionospheric dynamo that generates the *Sq* geomagnetic field is extremely complex. In the ionospheric dynamo region, the plasma flow, driven by the collisions between neutral and charged particles (Vasyliūnas, 2012; Yamazaki and Maute, 2017), produces an electric field, which in turn leads to the magnetic field perturbation according to the Faraday's law. The deformation of the magnetic field perturbation again produces the ionospheric currents through the Ampère's law that generate the *Sq* and other daily variations of geomagnetic field. As the timescale of geomagnetic field modeling is much longer than the ionospheric response time, the steady state assumption is valid, under which the electric field and currents in the E-region are in equilibrium with the velocity of neutral wind-driven motions. Consequently, both the electric field and the velocity of neutral wind that interacts with the background geomagnetic field in the ionosphere, where the electric conductivity is highly anisotropic, produce the ionospheric currents that result in the daily variations of geomagnetic field.

The neutral wind can be treated as tidal oscillations of the atmosphere, driven by the thermal forcing from the sun and the gravitational influences of the moon. In fact, atmospheric tides are coupled with the *Sq* and *L* variations. Kato (1956, 1957, 1966) found that the electric currents that generate the *Sq* geomagnetic field are mainly driven by the negative-mode diurnal tide. The *L* variations are related to the lunar tides (Campbell, 1980). The atmospheric tides are usually classified, at least, into semidiurnal, diurnal, seasonal, interannual and annual tides, each of which exhibits distinct temporary period and spatial structure (Forbes et al., 2008; England, 2012). The background geomagnetic field, that interacts with the velocity of neutral winds, is primarily dominated by the main field generated in the liquid core of Earth, and undergoes secular (Bloxham et al., 1989) and other variations. Since the atmospheric tides and the background geomagnetic field vary at various temporary and spatial scales, the resulted *Sq* geomagnetic field becomes extremely complex. Therefore, it's challenging to take into account the ionospheric dynamo process in high-precision geomagnetic field modeling.

Based on the thin layer assumption, the classic tide theory (Siebert, 1961; Lindzen and Chapman, 1969) has been successfully applied for the explanation of tide-related phenomenon in the Earth's atmosphere. Besides, the electrodynamics of atmosphere (Volland, 1984) has revealed the physical mechanism of the generation of the complex current systems in the ionosphere. By integrating the classical tide theory with the atmospheric electrodynamics, this research is dedicated to developing a model that concerns the physical mechanism of the generation of *Sq* geomagnetic field by the interaction between the atmospheric tides and the background magnetic field in the ionosphere. Other daily variations concerning the electric field, induction in the upper mantel, EEJ or *L* will not be investigated in this research. This physical model has the potential of enhancing the precision of geomagnetic field modeling for the MSS-1 mission.

In what follows, the construction of the velocity of atmospheric tides and the theory of generating the *Sq* geomagnetic field by the tidal motions are introduced in Section 2. Based on it, some results of the application of this newly developed model on MSS-1 data are in Section 3. Finally, Section 4 summarizes this research and sets the goal for the further development of this physical model.

2. Method

2.1 The Classic Tide Theory

We utilize the classic tide theory (Siebert, 1961; Lindzen and Chapman, 1969) to model the tidal motions in the Earth's atmosphere, driven by both solar thermal forcing and the gravitational tidal effects of the moon. In the classic tide theory the atmosphere is simplified as a compressible ideal gas of single composition in a thin spherical layer, compared with the radius of Earth R_E = 6371.2 km. In the equilibrium state the spherically symmetric atmosphere requires:

$$\frac{\mathrm{d}p_0(z)}{\mathrm{d}z} = -\rho_0(z)g, \tag{1}$$

$$p_0(z) = \rho_0(z)RT_0(z), \tag{2}$$

$$p_0(z) = \rho_0(z)gH(z), \tag{3}$$

where $H(z)$ is the scale height, R is the gas constant, and the acceleration of gravity $\boldsymbol{g} = -g\hat{\boldsymbol{r}}$ is assumed to be constant, and p_0, ρ_0 and T_0 represent the pressure, density and temperature in the hydrostatic state, respectively. Here, z is the height of fluid parcels in the atmosphere with the radius being defined as $r = R_E + z$.

The classic tide theory further assumes that the Lorentz force is weaker than the Coriolis force while the viscous force is negligible. The atmosphere is also assumed to be in thermodynamic equilibrium during hydrodynamic evolutions. Consequently, the fluid dynamics of the atmosphere, to the leading-order approximation, is decoupled from the electromagnetic dynamics and is governed by the following equations:

$$\rho\left(\frac{\partial \boldsymbol{u}}{\partial t} + \boldsymbol{u}\cdot\nabla\boldsymbol{u} + 2\boldsymbol{\Omega}\times\boldsymbol{u}\right) = -\nabla p + \rho\boldsymbol{g} - \rho\nabla V_T, \tag{4a}$$

$$\frac{\partial \rho}{\partial t} + \nabla\cdot(\rho\boldsymbol{u}) = 0, \tag{4b}$$

$$\frac{\mathrm{d}p}{\mathrm{d}t} = \frac{\gamma p}{\rho}\frac{\mathrm{d}\rho}{\mathrm{d}t} + (\gamma-1)\rho J, \tag{4c}$$

in which $\boldsymbol{u} = w\hat{\boldsymbol{z}} + u\hat{\boldsymbol{\theta}} + v\hat{\phi}$ is the velocity, ρ denotes the density, p represents the pressure, t is time, $\boldsymbol{\Omega} = \Omega\hat{\boldsymbol{z}}$ is the constant angluar velocity of Earth, V_T is any tidal potential, J is the thermotidal heating per unit mass per unit time, and $\gamma = c_P/c_V$ is the adiabatic index with c_P and c_V being the specific heat of constant pressure and that of constant volume, respectively. In this article, $(\hat{\boldsymbol{x}}, \hat{\boldsymbol{y}}, \hat{\boldsymbol{z}})$ denote the orthogonal unit vectors in the Cartesian coordinates while $(\hat{\boldsymbol{r}}, \hat{\boldsymbol{\theta}}, \hat{\phi})$ represent those in the polar spherical coordinates.

With the equilibrium state defined by Equation (1), the physical fields in the atmosphere can be expanded as:

$$p = p_0(z) + \delta p(z, \theta, \phi, t), \tag{5a}$$

$$\rho = \rho_0(z) + \delta\rho(z, \theta, \phi, t), \tag{5b}$$

$$T = T_0(z) + \delta T(z, \theta, \phi, t), \tag{5c}$$

where δp, $\delta\rho$ and δT are perturbations caused by tidal motions. The gravitational perturbation is neglected, which is acceptable for atmospheric tides. Substitution of the expansions (5) into the governing Equations (4) gives rise to the perturbation equations that describe the tidal dynamics of atmosphere:

$$\frac{\partial \boldsymbol{u}}{\partial t} + 2\boldsymbol{\Omega}\times\boldsymbol{u} = -\frac{1}{\rho_0}\nabla\delta p + \frac{\delta\rho}{\rho_0}\boldsymbol{g} - \nabla V_T, \tag{6a}$$

$$\frac{\partial \delta\rho}{\partial t} + \boldsymbol{u}\cdot\nabla\rho_0 + \rho_0\nabla\cdot\boldsymbol{u} = 0, \tag{6b}$$

$$\frac{\partial \delta p}{\partial t} + \boldsymbol{u}\cdot\nabla p_0 = \gamma g H\left(\frac{\partial \delta\rho}{\partial t} + \boldsymbol{u}\cdot\nabla\rho_0\right) + (\gamma-1)\rho_0 J, \tag{6c}$$

where nonlinear and other higher-order terms have been neglected. According to scale analysis in dynamical meteorology at global length scale, vertical motions are much smaller than the horizontal ones, $w \ll u, v$. And as usual in geophysics, the traditional approximation (Eckart, 1960), i.e., neglecting the tangential component of the rotation vector $\boldsymbol{\Omega}$, is adopted in this research. Consequently from Equations (6), we obtain the full perturbation equations in the scalar form for tidal motions of the atmosphere:

$$\frac{\partial u}{\partial t} - 2\Omega v\cos\theta = -\frac{1}{R_\mathrm{E}}\frac{\partial}{\partial\theta}\left(\frac{\delta p}{\rho_0} + V_T\right), \tag{7a}$$

$$\frac{\partial v}{\partial t} + 2\Omega u\cos\theta = -\frac{1}{R_\mathrm{E}\sin\theta}\frac{\partial}{\partial\phi}\left(\frac{\delta p}{\rho_0} + V_T\right), \tag{7b}$$

$$\frac{\partial \delta p}{\partial z} = -g\delta\rho - \rho_0\frac{\partial V_T}{\partial z}, \tag{7c}$$

$$\frac{\partial \delta\rho}{\partial t} + w\frac{\mathrm{d}\rho_0}{\mathrm{d}z} + \rho_0\chi = 0, \tag{7d}$$

$$\chi = \frac{1}{R_\mathrm{E}\sin\theta}\frac{\partial}{\partial\theta}(u\sin\theta) + \frac{1}{R_\mathrm{E}\sin\theta}\frac{\partial v}{\partial\phi} + \frac{\partial w}{\partial z}, \tag{7e}$$

$$\frac{\partial \delta p}{\partial t} + w\frac{\mathrm{d}p_0}{\mathrm{d}z} = \gamma g H\left(\frac{\partial \delta\rho}{\partial t} + w\frac{\mathrm{d}\rho_0}{\mathrm{d}z}\right) + (\gamma-1)\rho_0 J, \tag{7f}$$

where θ denotes the colatitude and ϕ represents the longitude.

As we are interested in periodically tidal motions in time and longitude, a physical field F we are concerned with is converted into the new form:

$$F(z,\theta,\phi,t) = F^{\sigma,m}(z,\theta)\,\mathrm{e}^{\mathrm{i}(m\phi+\sigma t)}, \tag{8}$$

where $\mathrm{i} = \sqrt{-1}$ is the imaginary unit, m denotes the azimuthal wavenumber, and σ represents the angular frequency of tidal motions. Now we introduce the meteorological vertical speed:

$$G = -\frac{1}{\gamma p_0}\left(\frac{\partial \delta p}{\partial t} + w\frac{\mathrm{d}p_0}{\mathrm{d}z}\right). \tag{9}$$

After some mathematical manipulations, Equations (2), (3) and (7) lead to a single equation for $G^{\sigma,m}$:

$$H\frac{\partial^2 G^{\sigma,m}}{\partial z^2} + \left(\frac{\mathrm{d}H}{\mathrm{d}z} - 1\right)\frac{\partial G^{\sigma,m}}{\partial z} = \frac{g}{4R_\mathrm{E}^2\Omega^2}\mathcal{F}\left[\left(\frac{\mathrm{d}H}{\mathrm{d}z} + \kappa\right)G^{\sigma,m} - \frac{\kappa J^{\sigma,m}}{\gamma g H}\right], \tag{10}$$

where $\kappa = (\gamma-1)/\gamma$, and the operator is defined by:

$$\mathcal{F} = \frac{1}{\sin\theta}\frac{\partial}{\partial\theta}\left(\frac{\sin\theta}{f^2-\cos^2\theta}\frac{\partial}{\partial\theta}\right) - \frac{1}{f^2-\cos^2\theta}\left(\frac{m}{f}\frac{f^2+\cos^2\theta}{f^2-\cos^2\theta} + \frac{m^2}{\sin^2\theta}\right), \tag{11}$$

and a term associated with the variation of ${V_T}^{\sigma,m}$ with respect to the height z has been neglected as the vertical length scale of ${V_T}^{\sigma,m}$ is much larger than the thickness of the thin atmosphere layer. We may assume a function $F^{\sigma,m}$, such as $G^{\sigma,m}$ and $J^{\sigma,m}$, can be expanded as:

$$F^{\sigma,m}(z,\theta) = \sum_n F_n^{\sigma,m}(z)\Theta_n^{\sigma,m}(\theta). \tag{12}$$

By the method of separation of variables, Equation (10) can be separated into the horizontal and vertical parts:

$$\mathcal{F}(\Theta_n^{\sigma,m}) = -\lambda_n^{\sigma,m}\Theta_n^{\sigma,m}, \tag{13a}$$

$$H\frac{\mathrm{d}^2 G_n^{\sigma,m}}{\mathrm{d}z^2} + \left(\frac{\mathrm{d}H}{\mathrm{d}z} - 1\right)\frac{\mathrm{d}G_n^{\sigma,m}}{\mathrm{d}z} + \frac{1}{h_n^{\sigma,m}}\left(\frac{\mathrm{d}H}{\mathrm{d}z} + \kappa\right)G_n^{\sigma,m} = \frac{\kappa}{\gamma g H h_n^{\sigma,m}}J_n^{\sigma,m}, \tag{13b}$$

where the constant of separation $h_n^{\sigma,m}$ is called the equivalent depth and $\lambda_n^{\sigma,m} = 4R_\mathrm{E}^2\Omega^2/(gh_n^{\sigma,m})$. Equation (13a) is the famous Laplace tidal equation that governs the horizontal structures of tidal motions. Hough (1897) first systematically studied the solutions of this eigenvalue problem Equation (13a) by the method of spherical harmonic expansion. As a result the eigenfunctions $\Theta_n^{\sigma,m}$ are also called the Hough functions. The orthogonality and completeness of the Hough functions have been proved by Lindzen and Chapman (1969) and Holl (1970). The classic tide theory has shown that the velocity components of tidal motions governed by Equations (7) can be expanded as:

$$w^{\sigma,m}(z,\theta) = \sum_n w_n^{\sigma,m}(z)\Theta_n^{\sigma,m}(\theta), \tag{14a}$$

$$u^{\sigma,m}(z,\theta) = \sum_n u_n^{\sigma,m}(z)U_n^{\sigma,m}(\theta), \tag{14b}$$

$$v^{\sigma,m}(z,\theta) = \sum_n v_n^{\sigma,m}(z)V_n^{\sigma,m}(\theta), \tag{14c}$$

where $U_n^{\sigma,m}(\theta)$ and $V_n^{\sigma,m}(\theta)$ are defined by:

$$U_n^{\sigma,m}(\theta) = \frac{1}{f^2-\cos^2\theta}\left(\frac{\mathrm{d}\Theta_n^{\sigma,m}}{\mathrm{d}\theta} + \frac{m}{f}\frac{\cos\theta}{\sin\theta}\Theta_n^{\sigma,m}\right), \tag{15a}$$

$$V_n^{\sigma,m}(\theta) = \frac{1}{f^2-\cos^2\theta}\left(\frac{\cos\theta}{f}\frac{\mathrm{d}\Theta_n^{\sigma,m}}{\mathrm{d}\theta} + \frac{m}{\sin\theta}\Theta_n^{\sigma,m}\right), \tag{15b}$$

and functions $w_n^{\sigma,m}(z)$, $u_n^{\sigma,m}(z)$ and $v_n^{\sigma,m}(z)$ are determined by the $G_n^{\sigma,m}(z)$ of Equation (13b), which will not be discussed in this research.

2.2 The *Sq* Geomagnetic Field Model

The *Sq* geomagnetic field is generated by the electric field and currents in the E-region of ionosphere, driven by the tidal motions of atmosphere, whose thickness is negligible compared with the radius R_E of Earth. Therefore, in our physical model the vertical variations of the tidal motions, responsible for the *Sq* geomagnetic field, are neglected in the thin ionospheric layer. Then the tidal motions are parameterised on the spherical surface $\mathcal{S}$ of height z = 110 km above the ground, according to Equations (14), as:

$$w(\theta,\phi,t) = \sum_{\sigma,m,n}\Theta_n^{\sigma,m}(\theta)\left[a_{n,c}^{\sigma,m}\cos(m\phi+\sigma t) + a_{n,s}^{\sigma,m}\sin(m\phi+\sigma t)\right], \tag{16a}$$

$$u(\theta,\phi,t) = \sum_{\sigma,m,n}U_n^{\sigma,m}(\theta)\left[a_{n,c}^{\sigma,m}\cos(m\phi+\sigma t) + a_{n,s}^{\sigma,m}\sin(m\phi+\sigma t)\right], \tag{16b}$$

$$v(\theta,\phi,t) = \sum_{\sigma,m,n}V_n^{\sigma,m}(\theta)\left[a_{n,c}^{\sigma,m}\cos(m\phi+\sigma t) + a_{n,s}^{\sigma,m}\sin(m\phi+\sigma t)\right]. \tag{16c}$$

The tidal motions in the ionosphere are parameterized by the coefficients $a_{n,c}^{\sigma,m}$ and $a_{n,s}^{\sigma,m}$ to be determined from the geomagnetic observations. As the priority of this research is to set a framework in which the *Sq* geomagnetic field can be separated from the MSS-1 measurements, it is acceptable and practical to neglect the variations of the vertical structures of tidal motions. However, this simplification might distort the inverted tidal motions. For example, as the propagation of tidal waves and energy is deeply influenced by the vertical structure of atmospheric tides, the inverted tidal motions in our model cannot accurately capture the dynamics of tidal waves.

With the atmospheric tide model Equation (16) and assuming that the electromagnetic process is decoupled from the tidal motions, the height-integrated electric currents due to the tidal motions are represented, according to the Ohm's law, by (Volland, 1984, 1995; Yamazaki and Maute, 2017):

$$\boldsymbol{J} = \sigma_P(\boldsymbol{u}\times\boldsymbol{B}_0) + \sigma_H\frac{\boldsymbol{B}_0}{|\boldsymbol{B}_0|}\times(\boldsymbol{u}\times\boldsymbol{B}_0), \tag{17}$$

in which σ_P and σ_H denote the height-integrated Pedersen and Hall conductivities, respectively, and $\boldsymbol{B}_0$ represents the background geomagnetic field. Here, we have temporarily neglected the electric field in this research. The horizontal component $\boldsymbol{J}_H$ of the height-integrated electric currents is usually linked to a current function

$$\boldsymbol{J}_H = \nabla\times(\Psi\hat{\boldsymbol{r}}), \tag{18}$$

defined on the spherical surface of $\mathcal{S}$. The *Sq* geomagnetic field generated by the height-integrated electric currents $\boldsymbol{J}$, via the Biot–Savart law, is approximately to be:

$$\boldsymbol{B}(\boldsymbol{r},t) \approx \frac{\mu_0}{4\pi}\int_{\mathcal{S}}\boldsymbol{J}(\boldsymbol{r}',t)\times\frac{\boldsymbol{r}-\boldsymbol{r}'}{|\boldsymbol{r}-\boldsymbol{r}'|^3}\,\mathrm{d}\mathcal{S}', \tag{19}$$

in which μ_0 is the magnetic constant, and the vectors $\boldsymbol{r}'$ and $\boldsymbol{r}$ mark the positions of the height-integrated electric currents in the ionosphere and the *Sq* geomagnetic field, respectively. In practice, only the contributions of $\boldsymbol{J}$ to the *Sq* geomagnetic field within the part of the spherical surface $\mathcal{S}$, where $|\boldsymbol{r}-\boldsymbol{r}'| < |\boldsymbol{r}|$, are considered. Contributions from other regions of $\mathcal{S}$ are assumed to be negligible due to the long distance and Earth's shielding effects. For the sake of simplification, the background geomagnetic field $\boldsymbol{B}_0$ is provided by the core field of the CHAOS–8 model (Kloss et al., 2024) in this research.

For the given values of an azimuthal wavenumber m and an angular frequency σ, there exists infinitely many pairs of the eigenfunctions $\Theta_n^{\sigma,m}$ and eigenvalues $\lambda_n^{\sigma,m}$ that are satisfied with the eigenvalue problem (Equation (13a)). Following Flattery (1967)'s notation, we define an integer $l \equiv |n| - |m|$ with $l \geq 0$ for $|m| > 0$ or $l \geq 1$ for $m = 0$ (Miles, 1977), then the number of zeros of $\Theta_n^{\sigma,m}(n > 0)$ in $-1 < \cos\theta < 1$ is l while the number of zeros of $\Theta_n^{\sigma,m}(n < 0)$ is either $l + 1$ for even l or $l - 1$ for odd l; if all eigenvalues are positive for given σ and m, both the equatorially symmetric and anti-symmetric Hough functions are ordered together with positive n; if the eigenvalues can be either positive or negative, the equatorially symmetric and anti-symmetric Hough functions are ordered separately, with positive $n > 0$ corresponding to Hough funtions with positive eigenvalues while negative $n < 0$ corresponding to the Hough functions with negative eigenvalues.

In practice, only the Hough functions with small enough absolute eigenvalues correspond to large scale tidal motions, which can be easily obtained via numerical computation using normalized associated Legendre polynomial expansion (Groves, 1981; Wang YB et al., 2016). In order to model the daily variations of geomagnetic field, in our model we only temporarily consider about tidal motions with periods T of 6, 8, 12 and 24 hours. The angular frequencies of the tidal motions and parameters f are then determined as $\sigma = 2\pi/T$ and $f = 12/T$, respectively. As we are concerned with large-scale tidal motions, the azimuthal wavenumber m is truncated at maximum order 3 for each period T. As the current function has two vortex structures that are approximately symmetric about the equator, only the equatorially symmetric Hough functions are adopted in the construction of velocity Equation (16) of the tidal motions. Moreover, for a given period T and azimuthal wavenumber m, as illustrated in Figure 1, the Hough functions that have 0 or 1 root except the poles in each hemisphere are selected for Equation (16). When the small-scale structures are taken into consideration in further research, the Hough functions of higher order and with more roots will be included in our model. As the MSS-1 does not provide measurements at high latitudes, the Hough functions with negative eigenvalues and more roots, which are highly oscillating in polar regions, shall be carefully excluded from the model. Otherwise, the *Sq* geomagnetic field is distorted in polar regions. Under these criteria, a total of 35 Hough functions are included in Equation (16), requiring only 70 coefficients to be determined in the inversion.

3. Results

We assessed the performance of our *Sq* geomagnetic field model

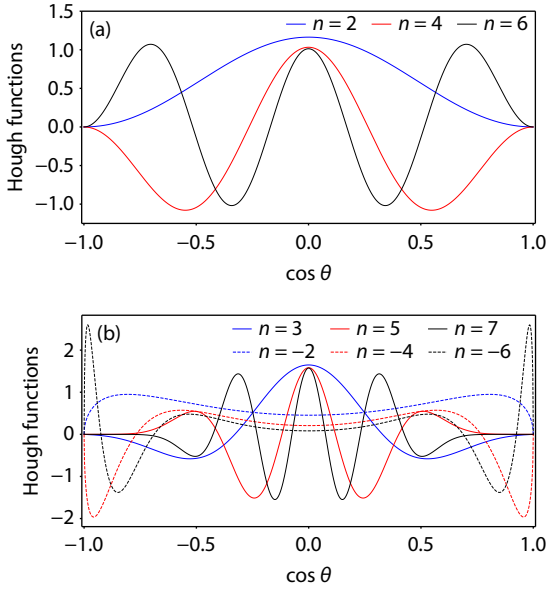

Figure 1. Equatorially symmetric Hough functions of different periods and azimuthal wavenumbers. The eigenvalues $\lambda_n^{\sigma,m}$ are all positive for $T = 1/2$, $f = 1$, and $m = 2$ in panel (a) while the eigenvalues can be either positive or negative for $T = 1$, $f = 0.5$ and $m = 1$ in panel (b). The solid lines correspond to Hough functions with positive eigenvalues while the dashed lines depict those with negative eigenvalues. Only the Hough functions with $n = 2, 4$ in panel (a) and $n = -2, 3, -4$ in panel (b) are selected for computation.

using a dataset comprising 5000 samples from the MSS-1 measurements provided by Yao HB et al. (2025c), in which the selection criteria on data are listed in detail. These measurements were collected over a span of approximately 18 days, starting from around $t = 8706$ days (MJD2000, October 23, 2023) to $t = 8723$ days (MJD2000, November 9, 2023). The contributions from the Earth's liquid core, mantle and curst, magnetosphere, and ocean tides have been subtracted from the data using the MGFM geomagnetic field model (Yao HB et al., 2025c). The inversion of the coefficients $a_{n,c}^{\sigma,m}$ and $a_{n,s}^{\sigma,m}$ in Equation (16) from the data is a linear and overdetermined problem. The general least-squares approach was adopted to tackle this inversion problem. Our model relies on the quality of the height-integrated conductivity model, which is highly anisotropic in space and dichotomic between the dayside and nightside of Earth. We synthesized a model for the height-integrated Pedersen σ_P and Hall σ_H conductivities (Figure 2) from the International Reference Ionosphere model (Bilitza et al., 2022). Our conductivity model is in fact derived from the global distribution of the height-integrated conductivities from the 90 km to 150 km above the ground at beginning of November, 2023. The deviations of the real height-integrated electric conductivities from the synthetic model are neglected during the short period of measurements.

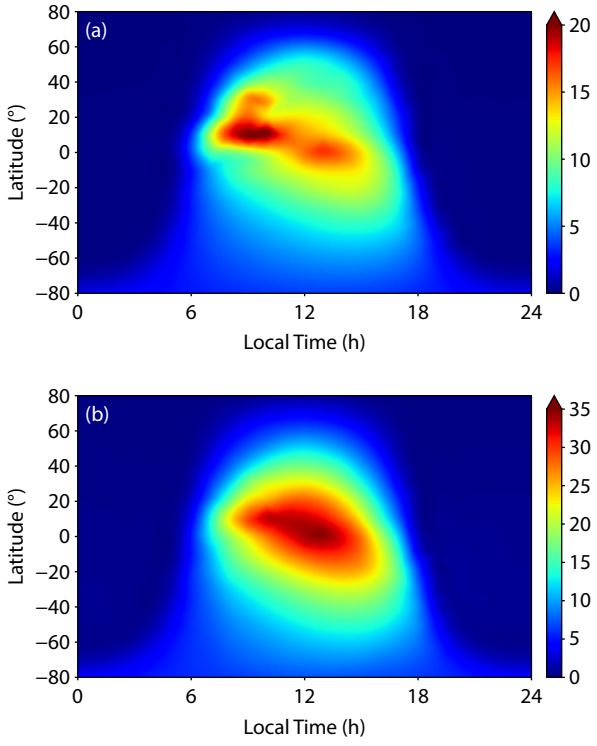

Figure 2. The synthetic model of the height-integrated Pedersen (a) and Hall (b) conductivities (S).

Figure 3 exhibits the inversion results of the *Sq* geomagnetic field. Compared with the MSS-1 observations, it is demonstrated that the inversion results of the *Sq* geomagnetic field provided by our model reflect the main feature of the MSS-1 observations. The root mean square (RMS) value of the observations is 7.79 nT, while the RMS of the misfit after extracting the model results from data is reduced to 6.60 nT. This shows that our model can effectively detect the ionospheric *Sq* magnetic field out of the total geomagnetic field measurements of the MSS-1 mission. The remaining misfit mainly comes from the $\hat{\phi} \cdot \boldsymbol{B}$ component of the geomagnetic field between the observations and inversion results. This could be caused by the oversimplification of the electric current density model and the height-integrated electric conductivity model.

Figure 4 displays the inversion results of the coefficients $a_{n,c}^{\sigma,m}$ and $a_{n,s}^{\sigma,m}$ of velocity field of the atmospheric tides in Equation (16). The values of all coefficients and the parameters of related tidal modes are also listed in Table 1. Among all the 35 tidal modes $(\Theta_n^{\sigma,m}, U_n^{\sigma,m}, V_n^{\sigma,m})$, the one that has the largest coefficients in absolute size is the diurnal mode with $m = 0$ and $n = 0$, followed by the semi-diurnal mode with $m = 0$ and $n = 0$. Another two tidal modes

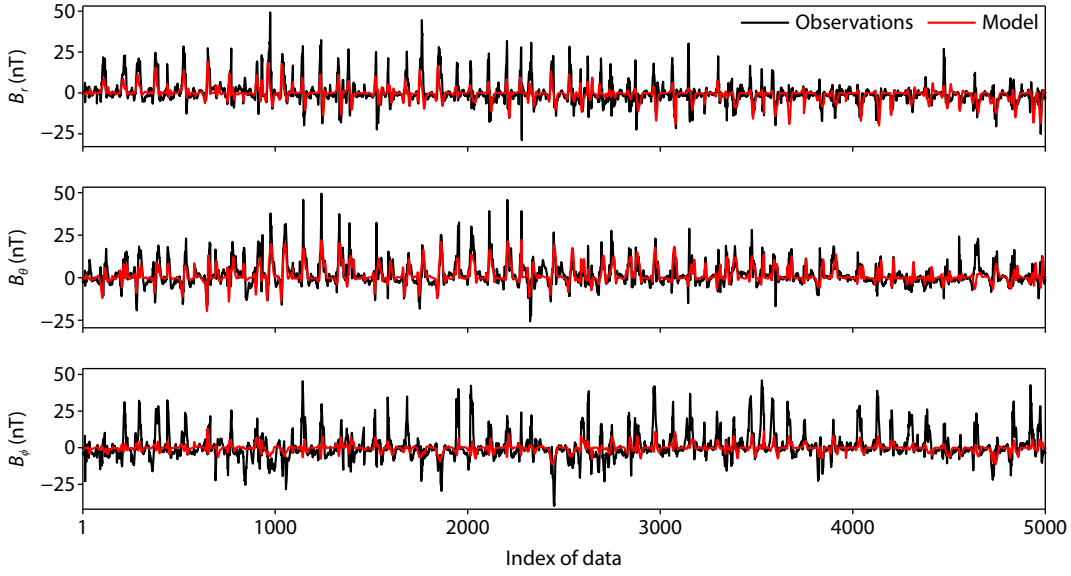

Figure 3. Comparison of the geomagnetic field between the MSS-1 observations and inversion results by our *Sq* geomagnetic field model. The black curves represent the MSS-1 observations while the red curves depict the inversion results of the *Sq* geomagnetic field model.

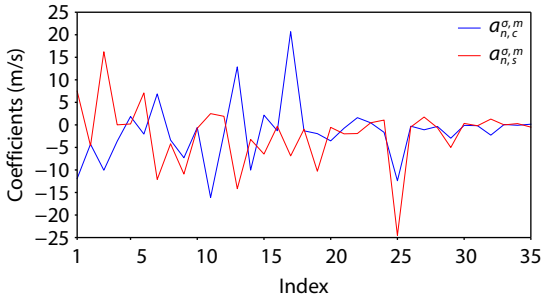

Figure 4. The coefficients of velocity field of the atmospheric tides inverted from the MSS-1 data.

of $m = 2$ and $n = 2$ with $T = 8$ hours and $m = 1$ and $n = 1$ with $T = 6$ hours contribute significantly to the atmospheric tides as well. The coefficients of the negative diurnal modes ($n < 0$) are relatively negligible in our *Sq* geomagnetic field model. But this does not mean that these negative diurnal modes are physically insignificant. Since the tidal modes ($U_n^{\sigma,m}, V_n^{\sigma,m}, \Theta_n^{\sigma,m}$) are not orthogonal, i.e.,

$$\int_0^{\pi}\left[U_n^{\sigma,m}U_{n'}^{\sigma,m}+V_n^{\sigma,m}V_{n'}^{\sigma,m}+\Theta_n^{\sigma,m}\Theta_{n'}^{\sigma,m}\right]\sin\theta\,\mathrm{d}\theta\neq 0, \tag{20}$$

for $n \neq n'$, the size of the coefficients $a_{n,c}^{\sigma,m}$ and $a_{n,s}^{\sigma,m}$ does not directly indicate the energy of tidal modes. At $m = 0$ the Hough functions $\Theta_0^{\sigma,0}$ are constant for any temporary periods with all eigenvalues degenerating to zero, i.e., $\lambda_0^{\sigma,0} = 0$. Consequently, the associated horizontal modes disappear, i.e., $U_0^{\sigma,0} = 0$ and $V_0^{\sigma,0} = 0$. Hence, it is not demonstrated that the tidal modes at $m = 0$ are physically significant even when their coefficients are large in absolute size. The missing zonal rotational modes at $m = 0$ were also discussed in a shallow-water model by Swarztrauber and Kasahara (1985).

With the coefficients in Table 1, we can obtain the current function Ψ defined in Equation (18). Figure 5 shows the normalized current function on October 24, 2023 at 110 km in altitude. There is clearly a pair of vortex structures in Ψ nearly symmetric about the equator on the dayside of Earth. One vortex counterclockwise in the Northern hemisphere and the other clockwise in the Southern hemisphere. Figure 6 shows the radial component $\hat{\boldsymbol{r}}\cdot\boldsymbol{B}$ of the related *Sq* geomagnetic field at 400 km above the ground at the same time of Figure 5, based on the results of inversion of MSS-1 data. The *Sq* geomagnetic field concentrates at places at which the vortex structures of the current function stay. It is also demonstrated that the *Sq* geomagnetic field in our model is also higly affected by the anisotropy and dichotomy of the electric conductivities in the ionosphere.

Table 1. Coefficients of tidal motions inverted from the MSS-1 data.

T (hour)	m	n	$a_{n,c}^{\sigma,m}$(m/s)	$a_{n,s}^{\sigma,m}$(m/s)	Index
6	0	0	−11.9042	7.4923	1
	0	2	−4.2798	−4.6313	2
	1	1	−10.0576	16.2278	3
	1	3	−3.6336	0.0086	4
	2	2	1.8644	0.2034	5
	2	4	−2.0370	7.0975	6
	3	3	6.8790	−12.1086	7
	3	5	−3.3688	−4.1919	8
8	0	0	−7.2968	−10.9121	9
	0	2	−0.5884	−0.7531	10
	1	1	−16.1190	2.5013	11
	1	3	−1.9162	1.9037	12
	2	2	12.8763	14.1612	13
	2	4	−10.0370	−3.2167	14
	3	3	2.1648	−6.4717	15
	3	5	−1.3029	−0.2984	16
12	0	0	20.6897	−6.8731	17
	0	2	−1.3120	−0.9732	18
	1	1	−1.9377	−10.2802	19
	1	3	−3.5475	−0.5488	20
	2	2	−0.7423	−1.9858	21
	2	4	1.6044	−1.9186	22
	3	3	0.4602	0.4730	23
	3	5	−1.6520	1.0711	24
24	0	0	−12.3996	−24.5178	25
	0	2	−0.2852	−0.4819	26
	0	−3	−1.0872	1.7450	27
	1	3	−0.3467	−0.6389	28
	1	−2	−2.9612	−5.0092	29
	1	−4	−0.1042	0.3302	30
	2	4	−0.1749	−0.1904	31
	2	−3	−2.2748	1.2919	32
	2	−5	0.0948	−0.0037	33
	3	3	−0.0895	0.2898	34
	3	−6	0.1530	−0.4946	35

4. Conclusions and Discussions

The *Sq* geomagnetic field is generated by the electric currents in the E-region of ionosphere driven by the atmospheric tides. With the classic tide theory, we have developed an *Sq* geomagnetic field model that reflects the physical mechanism of the ionospheric dynamo. Compared with other *Sq* geomagnetic field models, such as the DIFI chain algorithm which needs to deal with hundreds of parameters, in this model only a few parameters need to be determined from inversion. Besides, our model outputs the current function and the related *Sq* geomagnetic field that are satisfied with the physical expectation. Moreover, while other *Sq* geomagnetic field models do not concern the physical process of ionospheric dynamo, our model can provide with the tidal information that drives the ionospheric dynamo. This could help reveal the relations between the atmospheric tides and daily variations of geomagnetic field. However, the performance of our *Sq* geomagnetic field model is highly influenced by the electric conductivity models, which are still poorly investigated. The tidal modes

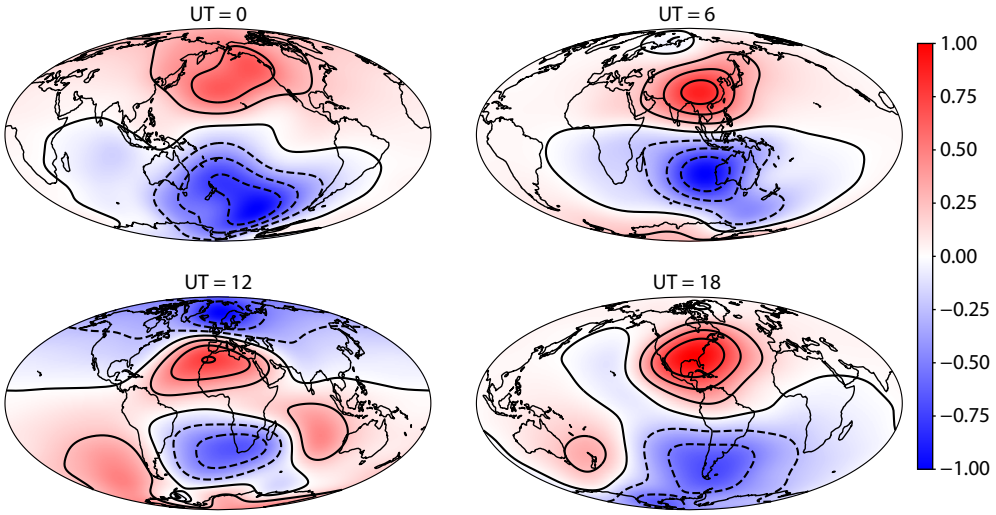

Figure 5. The normalized current function related to the *Sq* geomagnetic field on October 24, 2023 at 110 km in altitude.

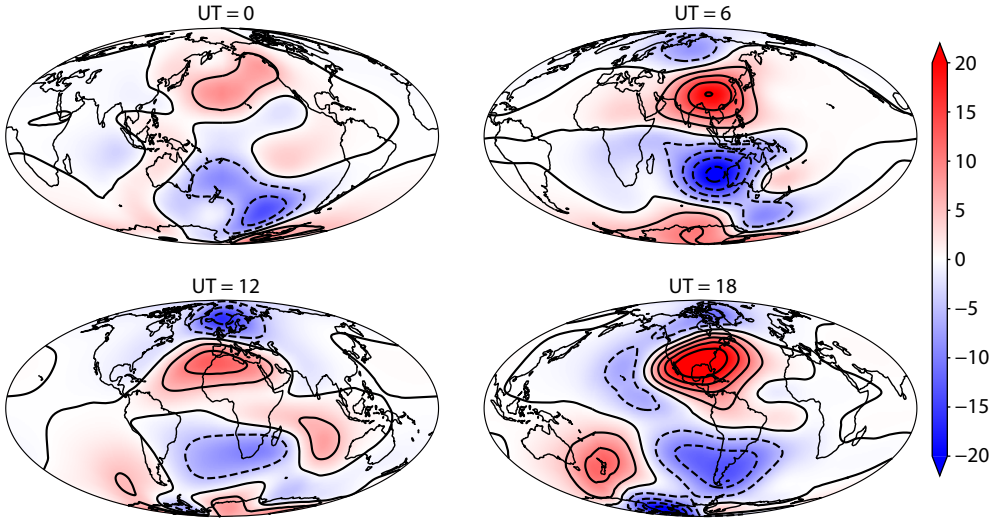

Figure 6. Contours of the radial component $\hat{\boldsymbol{r}} \cdot \boldsymbol{B}$ of *Sq* geomagnetic field (nT) at an altitude of 400 km above the Earth's surface. The data correspond to October 24, 2023.

$(U_n^{\sigma,m}, V_n^{\sigma,m}, \Theta_n^{\sigma,m})$ are not complete and orthogonal, the size of coefficients $a_{n,c}^{\sigma,m}$ and $a_{n,s}^{\sigma,m}$ cannot quantitatively indicate the energy of different tidal modes. We will also need to take care of the missing zonal rotational modes at $m = 0$ (Swarztrauber and Kasahara, 1985) because of the degeneracy of Laplace's tidal equation in the future. Nevertheless, our *Sq* geomagnetic field model could be used for the separation of the *Sq* geomagnetic field from the MSS-1 measurements, improving the accuracy of geomagnetic field modeling.

For practical usage and application, other contributions from the static electric field, EEJ, *L* variation, and induced currents in the upper mantle must be integrated in our model. The quality of our model is highly influenced by the electric conductivity model of ionosphere. Some more realistic conductivity models could be incorporated in the model to improve the precision of geomagnetic field modeling. As more data are used for inversion, long-term tides of monthly, seasonal, interannual and annual peiods must be considered in geomagnetic field modeling. The selection and symmetricity of tide modes could affect the inversion results in our model. The vertical structures of tides are not considered under the thin layer assumption, however, its justification and consequence need further investigation. These questions need to be addressed in future research.

Acknowledgments

This work is supported by the National Natural Science Foundation of China (Grant Nos. 12250013, 12403070, 12425306, 42250101, 12273092), the Macao Foundation, and Shanghai Post-doctoral Excellence Program (Grant No. 2023000137). The MSS-1 geomagnetic data are available at https://mss.must.edu.mo/data.html. The computation made use of the high performance computing resources in the Core Facility for Advanced Research Computing at Shanghai Astronomical Observatory, Chinese Academy of Sciences.

References

Bilitza, D., Pezzopane, M., Truhlik, V., Altadill, D., Reinisch, B. W., and Pignalberi,

A. (2022). The International Reference Ionosphere model: A review and description of an ionospheric benchmark. *Rev. Geophys.*, *60*(4), e2022RG000792. https://doi.org/10.1029/2022RG000792

Bloxham, J., Gubbins, D., and Jackson, A. (1989). Geomagnetic secular variation. *Philos. Trans. R. Soc. Lond. A, Math. Phys. Sci.*, *329*(1606), 415–502. https://doi.org/10.1098/rsta.1989.0087

Campbell, W. H. (1980). Annual and semiannual variations of the lunar semidiurnal geomagnetic field components at North American locations. *J. Geomagn. Geoelectr.*, *32*(2), 105–128. https://doi.org/10.5636/jgg.32.105

Campbell, W. H. (1989). An introduction to quiet daily geomagnetic fields. *PAGEOPH*, *131*(3), 315–331. https://doi.org/10.1007/BF00876831

Chapman, S. (1951). The equatorial electrojet as detected from the abnormal electric current distribution above Huancayo, Peru, and elsewhere. *Arch. Met. Geoph. Biokl. A*, *4*(1), 368–390. https://doi.org/10.1007/BF02246814

Chulliat, A., Vigneron, P., Thébault, E., Sirol, O., and Hulot, G. (2013). *Swarm* SCARF dedicated ionospheric field inversion chain. *Earth Planets Space*, *65*(11), 1271–1283. https://doi.org/10.5047/eps.2013.08.006

Chulliat, A., Vigneron, P., and Hulot, G. (2016). First results from the swarm dedicated ionospheric field inversion chain. *Earth Planets Space*, *68*(1), 104. https://doi.org/10.1186/s40623-016-0481-6

Eckart, C. (1960). *Hydrodynamics of Oceans and Atmospheres*. Oxford: Pergamon Press.

Emmert, J. T., Richmond, A. D., and Drob, D. P. (2010). A computationally compact representation of Magnetic-Apex and Quasi-Dipole coordinates with smooth base vectors. *J. Geophys. Res.: Space Phys.*, *115*(A8), A08322. https://doi.org/10.1029/2010JA015326

England, S. L. (2012). A review of the effects of non-migrating atmospheric tides on the Earth's low-latitude ionosphere. *Space Sci. Rev.*, *168*(1), 211–236. https://doi.org/10.1007/s11214-011-9842-4

Flattery, T. W. (1967). Hough functions, Technical Report 21, Department of Geophysical Sciences. University of Chicago.

Forbes, J. M., Zhang, X., Pa lo, S., Russell, J., Mertens, C. J., and Mlynczak, M. (2008). Tidal variability in the ionospheric dynamo region. *J. Geophys. Res.: Space Phys.*, *113*(A2), A02310. https://doi.org/10.1029/2007JA012737

Groves, G. V. (1981). Notes on obtaining the eigenvalues of Laplace's tidal equation. *Planet. Space Sci.*, *29*(12), 1339–1344. https://doi.org/10.1016/0032-0633(81)90100-8

Holl, P. (1970). The completeness of the orthogonal system of the Hough functions. *Nachrichten der Akad. der Wissenschaften Gottingen*, *7*, 159–168.

Hough, S. S. (1897). On the application of harmonic analysis to the dynamical theory of the tides. Part II. On the general integration of Laplace's dynamical equations. *Proc. R. Soc. Lond.*, *62*, 209–210.

Kato, S. (1956). Horizontal wind systems in the ionospheric *E* region deduced from the dynamo theory of the geomagnetic S_q variation Part II. Rotating Earth. *J. Geomagn. Geoelectr.*, *8*(1), 24–37. https://doi.org/10.5636/jgg.8.24

Kato, S. (1957). Horizontal wind systems in the ionospheric *E* region deduced from the dynamo theory of the geomagnetic S_q variation Part IV. *J. Geomagn. Geoelectr.*, *9*(2), 107–115. https://doi.org/10.5636/jgg.9.107

Kato, S. (1966). Diurnal atmospheric oscillation: 1. Eigenvalues and Hough functions. *J. Geophys. Res.*, *71*(13), 3201–3209. https://doi.org/10.1029/JZ071i013p03201

Kloss, C., Finlay, C. C., Olsen, N., Tøffner-Clausen, L., Gillet, N., and Grayver, A. (2024). Chaos-8 geomagnetic field model. https://doi.org/10.5281/zenodo.13950013

Lindzen, R. S., and Chapman, S. (1969). Atmospheric tides. *Space Sci. Rev.*, *10*(1), 3–188. https://doi.org/10.1007/BF00171584

Matsushita, S. (1968). *Sq* and *L* current systems in the ionosphere. *Geophys. J. R. Astr. Soc.*, *15*(1-2), 109–125. https://doi.org/10.1111/j.1365-246X.1968.tb05751.x

Miles, J. W. (1977). Asymptotic eigensolutions of Laplace's tidal equation. *Proc. R. Soc. Lond. A. Math. Phys. Sci.*, *353*(1674), 377–400. https://doi.org/10.1098/rspa.1977.0040

Olsen, N., Friis-Christensen, E., Floberghagen, R., Alken, P., Beggan, C. D., Chulliat, A., Doornbos, E., Da Encarnação, J. T., Hamilton, B., … Visser, P. N. (2013). The *Swarm* satellite constellation application and research facility (SCARF) and *Swarm* data products. *Earth Planets Space*, *65*(11), 1189–1200. https://doi.org/10.5047/eps.2013.07.001

Ren, Z. Y., Xie, Y. F., Chen, C. J., Yao, H. B., Tang, J. T., and Zhang, K. (2025a). New insights into Earth's mantle conductivity and water distribution using the Macau Science Satellite-1 data. *Earth Planet. Phys.*, *9*(3), 595–606. https://doi.org/10.26464/epp2025003

Ren, Z. Y., Huang, Y. P., Yang, C., Chen, C. J., and Zhang, K. (2025b). Preliminary results suggest observations from Macau Science Satellite-1 system can improve knowledge of tidal-induced magnetic fields. *Earth Planet. Phys.*, *9*(3), 586–594. https://doi.org/10.26464/epp2025002

Richmond, A. D. (1995). Ionospheric electrodynamics using magnetic apex coordinates. *J. Geomagn. Geoelectr.*, *47*(2), 191–212. https://doi.org/10.5636/jgg.47.191

Sabaka, T. J., Tøffner-Clausen, L., Olsen, N., and Finlay, C. C. (2020). CM6: a comprehensive geomagnetic field model derived from both CHAMP and Swarm satellite observations. *Earth Planets Space*, *72*(1), 80. https://doi.org/10.1186/s40623-020-01210-5

Schmucker, U. (1970). An introduction to induction anomalies. *J. Geomagn. Geoelectr.*, *22*(1-2), 9–33. https://doi.org/10.5636/jgg.22.9

Siebert, M. (1961). Atmospheric tides. *Adv. Geophys.*, *7*, 105–187. https://doi.org/10.1016/S0065-2687(08)60362-3

Swarztrauber, P. N., and Kasahara, A. (1985). The vector harmonic analysis of Laplace's tidal equations. *SIAM J. Sci. Stat. Comput.*, *6*(2), 464–491. https://doi.org/10.1137/0906033

Vasyliūnas, V. M. (2012). The physical basis of ionospheric electrodynamics. *Ann. Geophys.*, *30*(2), 357–369. https://doi.org/10.5194/angeo-30-357-2012

Volland, H. (1984). *Atmospheric Electrodynamics*. Berlin, Heidelberg: Springer-Verlag. https://doi.org/10.1007/978-3-642-69813-2

Volland, H. (1995). *Handbook of Atmospheric Electrodynamics, Volume II*. Boca Raton: CRC Press.

Wang, H. J., Boyd, J. P., and Akmaev, R. A. (2016). On computation of Hough functions. *Geosci. Model Dev.*, *9*(4), 1477–1488. https://doi.org/10.5194/gmd-9-1477-2016

Wang, Y. B., Zhang, Y., Wang, Y. J., Liu, P. F., Cheng, J. X., Li, X. Z., Tang, K., Li, L. G., and Duan, X. W. (2023). Influences of various space current systems on the geomagnetic field in near-Earth space. *Earth Planet. Phys.*, *7*(1), 93–99. https://doi.org/10.26464/epp2023010

Yamazaki, Y., and Maute, A. (2017). Sq and EEJ–a review on the daily variation of the geomagnetic field caused by ionospheric dynamo currents. *Space Sci. Rev.*, *206*(1), 299–405. https://doi.org/10.1007/s11214-016-0282-z

Yao, H. B., Xu, J. Y., Jiang, Y., Yan, Q., Yin, L., and Liu, P. F. (2025a). Influence of different data selection criteria on internal geomagnetic field modeling. *Earth Planet. Phys.*, *9*(3), 541–549. https://doi.org/10.26464/epp2025013

Yao, H. B., Xu, J. Y., and Zhang, K. (2025b). A method for simultaneously determining Earth's magnetic field and mantle conductivity models using MSS-1 and Swarm satellite magnetic data. *Phys. Earth Planet. Inter.*, *358*, 107296. https://doi.org/10.1016/j.pepi.2024.107296

Yao, H. B., Xu, J. Y., Yang, C., Ren, Z. Y., and Zhang, K. (2025c). A multisource geomagnetic field model incorporating ocean circulation-induced magnetic field. *Earth Planet. Phys.*, *9*(3), 550–563. https://doi.org/10.26464/epp2025029

Zhang, K. (2023). A novel geomagnetic satellite constellation: Science and applications. *Earth Planet. Phys.*, *7*(1), 4–21. https://doi.org/10.26464/epp2023019